Protein Science (1997), 6:1084–1091. Cambridge University Press. Printed in the USA.

Energy profile of maltooligosaccharide permeation through maltoporin as derived from the structure and from a statistical analysis of saccharide-protein interactions

JOACHIM E.W. MEYER AND GEORG E. SCHULZ

Institut für Organische Chemie und Biochemie, Albert-Ludwigs-Universität, Albertstraße 21, 79104 Freiburg im Breisgau, Germany

(RECEIVED November 4, 1996; ACCEPTED January 14, 1997)

Abstract

The crystal structure of the maltodextrin-specific porin from *Salmonella typhimurium* ligated with a maltotrioside at the pore eyelet is known at 2.4 Å resolution. The three glucose units assume a conformation close to the natural amylose helix. The pore eyelet fits exactly the cross-section of a maltooligosaccharide chain and thus functions as a constraining orifice. The oligomer permeates the membrane by screwing along the amylose helix through this orifice. Because each glucose glides along the given helix, its interactions can be sampled at any point along the pathway. The interactions are mostly hydrogen bonds, but also contacts to aromatic rings at one side of the pore. We have derived the energy profile of a gliding maltooligosaccharide by following formation and breakage of hydrogen bonds and by assessing the saccharide-aromatics interactions from a statistical analysis of saccharide binding sites in proteins. The resulting profile indicates smooth permeation despite extensive hydrogen bonding at the orifice.

Keywords: permeation model, saccharide-aromatics interactions, saccharide binding sites, specific membrane channel, X-ray structure

Porins form passive channels in the outer membrane of Gram-negative bacteria, which are used for the uptake of nutrients and for the exchange of ions through this protective barrier (Nikaido, 1994). There exist general porins with wide channels that are open for polar compounds but closed for nonpolar ones (Schulz, 1993). Furthermore, there are specific porins, among them the (maltodextrin-specific) maltoporins (Thirion & Hofnung, 1972). Maltoporins allow for the uptake of linear maltodextrins, while their permeability for small compounds including ions is much lower than that of general porins (Luckey & Nikaido, 1980a, 1980b; Benz et al., 1986).

Several structures of general porins (Weiss et al., 1990; Cowan et al., 1992; Kreusch & Schulz, 1994) and two structures of maltoporins (Schirmer et al., 1995; Meyer et al., 1997) are known. The two maltoporins differ grossly with respect to their tentacles presented to the external medium, but they resemble each other closely in their regions facing the periplasm and at their specificity-defining orifices. Here, we use the structure of one of these maltoporins ligated with a bound maltotrioside (Meyer et al., 1997) for deriving an energy profile for the permeation of a maltooligosaccharide.

Two permeation types for oligomers are conceivable: First a "ratchet type" where the movement from one glucose to the next is hindered by a high energy barrier, and second a "slide type" where the oligomer can glide freely from one of its ends to the other. While a "ratchet type" would hinder permeation seriously, a "slide type" would involve significant energy steps only on initial association and final dissociation of the oligomer. Here, we demonstrate that in spite of its defined binding site, maltoporin belongs to the "slide type."

Results and discussion

Construction of the pore

Maltoporin from *Salmonella typhimurium* follows the general construction principles of porins (Fig. 1). It consists of a trimer of 18-stranded hollow β-barrels, where each barrel contains 427 amino acid residues. With an M_r of 48,022 this maltoporin is much larger than general porins (M_r around 32,000). Most of the mass differ-

Reprint requests to: Dr. Georg E. Schulz, Institut für Organische Chemie und Biochemie, Albertstr. 21, 79104 Freiburg im Breisgau, Germany; e-mail: schulz@bio5.chemie.uni-freiburg.de.

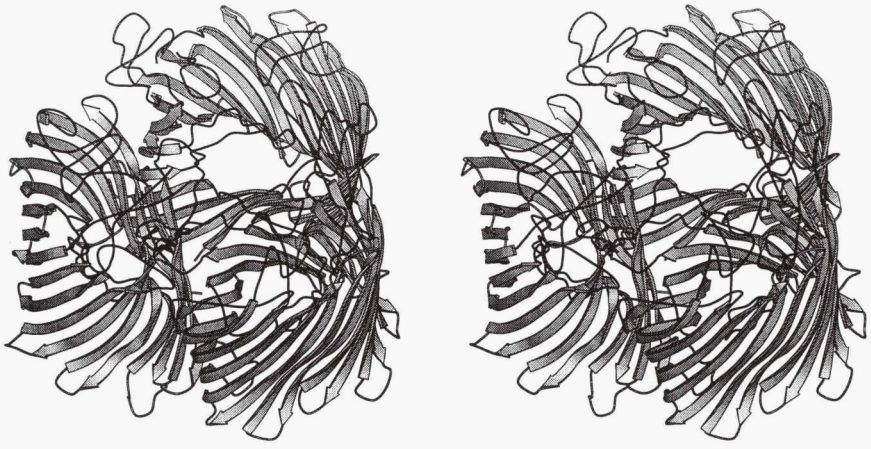

Fig. 1. Stereo view of trimeric maltoporin from *Salmonella typhimurium* consisting of three 18-stranded hollow β-barrels. The threefold axis is perpendicular to the membrane. Through each barrel runs a channel that is constricted to a small orifice in its middle.

ence lies in the large bulky tentacles of maltoporin, which protrude into the external medium, presumably fishing for maltodextrins.

The crystal structure of maltoporin from *S. typhimurium*, which had been ligated with p-nitrophenyl-maltotrioside by soaking for 2 days at a concentration of 5 mM, has been solved at 2.4 Å resolution (Meyer et al., 1997). The three glucose units of the ligand form a left-handed helix with the non-reducing end pointing towards the periplasm. The nitrophenyl group is located in the channel section opening to the external medium, but it is not visible indicating that its position is not defined. The result is in agreement with solution studies that revealed a maltooligosaccharide binding site in the pore with a dissociation constant somewhat below 1 mM (Schülein & Benz, 1990). The detailed binding structure is shown in Figure 2. The protein:ligand complex resembles the respective complex of the maltoporin from *Escherichia coli* (Dutzler et al., 1996).

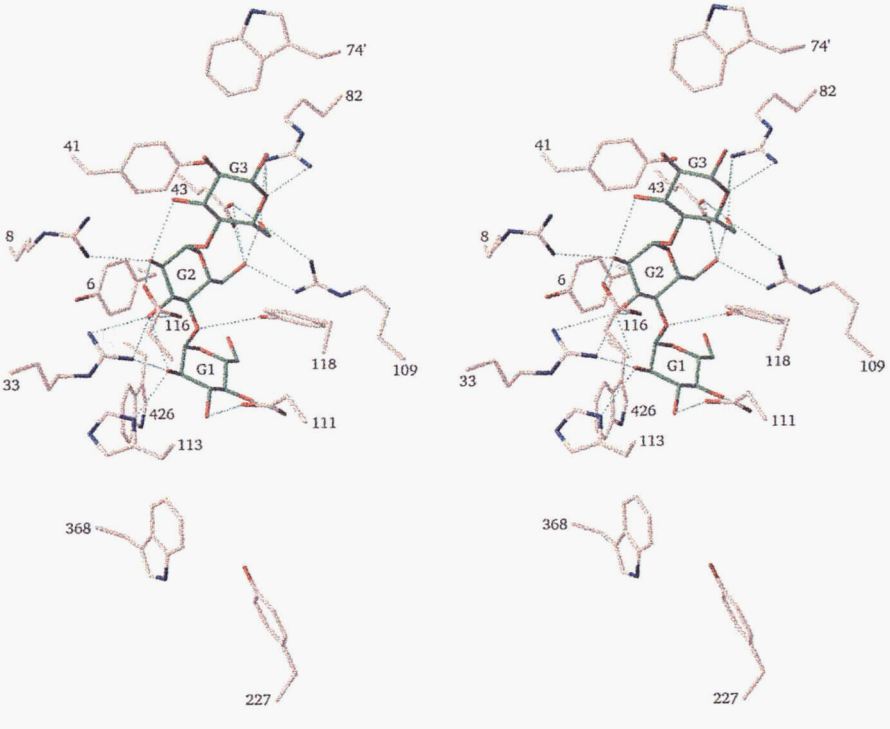

Fig. 2. Stereo view of a maltotrioside attached by numerous hydrogen bonds to the orifice of the maltoporin channel. The channel runs from the top (external medium) to the bottom (periplasm) and is lined by a ribbon of 6 aromatic side chains forming an irregular left-handed helix ("greasy slide," see text). The three glucose units G1, G2, and G3 make hydrophobic contacts to Trp426, Tyr6, and Tyr41, respectively.

Permeation geometry

The snug fit between the central glucose unit G2 of the maltotrioside and the constraining orifice is illustrated in Figure 3. The specificity of this pore is obvious. There are numerous hydrogen bonds between the glucose hydroxyl groups and polar residues (Fig. 2), and there is an additional nonpolar contact between the outer pyranose surface and Tyr6.

The bound maltotrioside consists of glucose units G1, G2 and G3 occupying sites S1, S2, and S3 of maltoporin. It fills the orifice and extends further into the wider channel sections above and below. The rotation/translation relation between glucose units G1 and G2 is almost identical to that between G2 and G3. The common relation can be used to extend the chain beyond both ends, giving rise to a regular helix with about 7 glucose units per turn at a pitch of 20 Å. This helix agrees well with the observations for single- and double-stranded amylose (Goldsmith et al., 1982; Hinrichs & Saenger, 1987).

Because of the well-fitting orifice (Fig. 3), the permeating chain has to proceed by a screwing motion along this helix, which transfers each glucose unit continuously from one of the observed positions S1, S2, and S3 to the next one. This regular helix can be followed for a total of five glucose units before clashes with the protein enforce deviations.

Hydrogen bonding of a permeating maltooligosaccharide

First we approximated the bound maltotriose by a regular glucose helix, which was subsequently used to model putative intermediate chain positions for determining the interactions in a continuous manner. For this purpose, the path between two glucose units was subdivided into ten equal steps. First, a single glucose unit was placed at each position, and all hydrogen bonds at the orifice were recorded. The polar interaction energy was taken as the sum of all hydrogen bond energies, where donor-acceptor distances below or equal 3.5, 3.1, and 2.7 Å were considered to contribute 1, 2, and 3 kJ/mol, respectively. The rough energy grading is supported by the quality of the structure, the energy scale is rather arbitrary but adjusted to approximate the observed dissociation constant of Schülein and Benz (1990). The evaluation scheme appears to be valid because there occurred only minor peptide conformational changes on maltotriose binding (Meyer et al., 1997).

The path of a single glucose, for instance G1, over the binding sites S3, S2, and S1 is sketched in Figure 4A. The resulting interaction profile (labeled G1) is shown in Figure 4B. The interaction is small when G1 reaches site S3, it is at its optimum shortly before S2, and it is small again at S1. Beyond S1 and beyond S3 we observed further hydrogen bonds giving rise to a constant basic interaction level of −4 kJ/mol. This level has been subtracted (to yield the profile of Fig. 4B) because it does not contribute to the points made.

The energy profile for an oligomer permeating the orifice can be derived by adding the contributions of single glucoses in proper register according to Figure 4A. The resulting interaction profile becomes periodic as soon as G1 passes over S1. The profile shows optimal binding always about 0.1 glucose units before the observed binding sites. It should be noted that the ripple on this profile amounts to merely ±10% of its depth.

Interactions with aromatic side chains

A peculiar feature of maltoporins is a ribbon of six aromatic side chains forming an irregular left-handed helix along the channel (Fig. 2), which has been dubbed "greasy slide" (Schirmer et al., 1995). Tyr41, Tyr6, and Trp426 of this ribbon are packed tightly edge to edge at the orifice and do contact the permeating pyranoses (see Fig. 3). There could be further contacts to the other aromatic side chains, but they are too weak for resulting in defined binding sites in the crystals (Dutzler et al., 1996; Meyer et al., 1997). The three aromatic rings at the orifice can be approximated by a left-

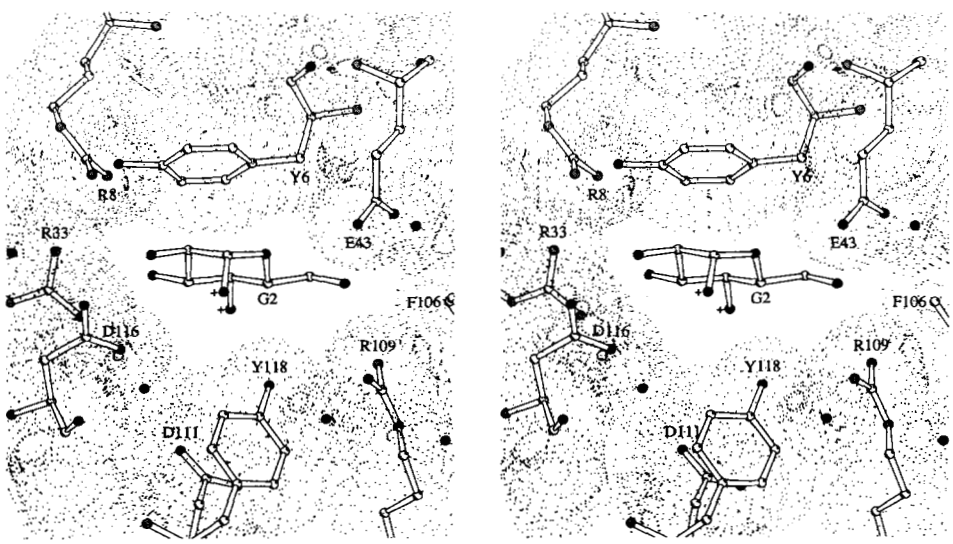

Fig. 3. Stereo view of the cross section of the channel orifice cut in parallel to the membrane plane. The molecular envelope was calculated according to Connolly (1993); it demonstrates the snug fit of a maltooligosaccharide, here glucose unit G2 of the bound maltotrioside. The glycosidic oxygens connecting adjacent units are marked by crosses. The upper surface of glucose unit G2, which is the outer surface of the saccharide helix, makes hydrophobic contacts with the aromatic ring of Tyr6. All other contacts are of a polar nature.

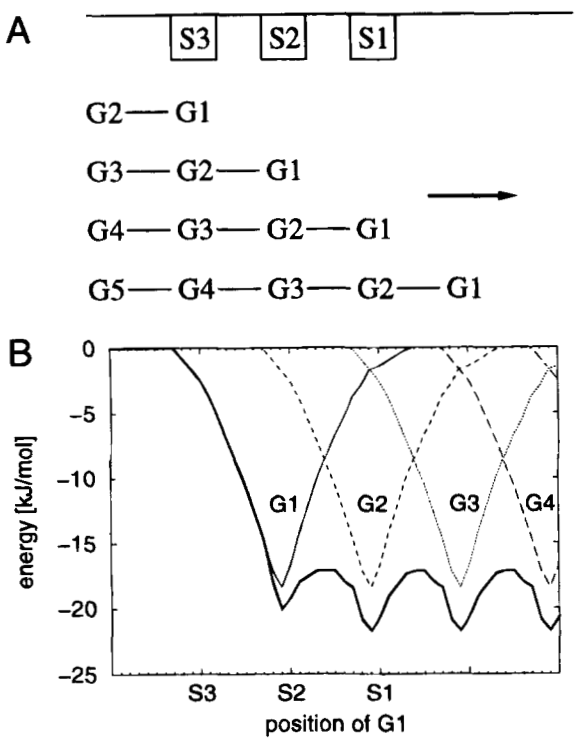

Fig. 4. Hydrogen bonding energy profile of a maltooligosaccharide screwing along the regular saccharide helix through the orifice of the maltoporin channel. **A:** Sketch of such an oligomer moving toward the periplasm and passing over sites S3, S2, and S1 that are outlined by the bound maltotrioside (Fig. 2). **B**: Energy profiles for glucose units G1, G2, etc., as they move over the binding sites. For a particular glucose unit, e.g., G1, the interactions are strongest when passing over S2 and much weaker at S3 and S1. The sum of all contributions (thick line) represents the total hydrogen bonding energy of a permeating oligomer. Note that the minimum for a maltotrioside is just before its observed position (G1 at S1, see Fig. 7).

handed helix similar to the glucose helix. The two helix axes, however, deviate by about 30° such that the permeation process cannot be described as one helix sliding along another one.

It is known that saccharide binding sites in proteins frequently contain aromatic side chains (Quiocho, 1989; Weis & Drickamer, 1996) pointing to a localized interaction between these partners. An attraction between the partial positive charges of the aliphatic hydrogens and the aromatic π-electrons is discussed (Chakrabarti & Samanta, 1995; Weis & Drickamer, 1996); but it should be rather weak because it does not enforce a defined ring packing arrangement (see below). Clearly, such binding sites are also favored by the hydrophobic effect.

The saccharide-aromatics interactions have to be clarified for the analysis of the permeation process, because it makes a difference whether the observed ribbon of aromatic side chains were a continuous "greasy slide" (Dutzler et al., 1996), or a row of separated attracting patches. In the absence of sufficient physicochemical data, we performed a statistical analysis of the observed saccharide binding sites and converted it to interaction energies.

Statistics of saccharide-binding sites in proteins

The Protein Data Bank (Bernstein et al., 1977) was screened for noncovalently bound pyranoses or oligomers thereof. Exclusion of all mutually homologous arrangements as well as all sialic acids and phosphorylated saccharides resulted in the 78 cases listed in Table 1. These demonstrate that pyranoses are predominantly bound at aromatic side chains (see Methods for the definition), in particular at tryptophans. In spite of the small sample, the preferences are significant. The subset of glucoses within the pyranoses has about half the size and distributes similarly (Table 1). The glucose distribution at tryptophans is shown in Figure 5.

A closer inspection showed that pyranoses tend to bind near to the aromatic ring centers, but there is neither a preferential saccharide orientation nor preferential interactions with the polar side chain atoms of tyrosines and tryptophans.

From frequencies to binding energies

Preferred pyranose binding at aromatic ring centers translates into an uneven profile of the saccharide-aromatic ring interaction energies for a maltooligosaccharide permeating maltoporin. For establishing this profile, we used the subset of glucoses binding at tyrosines as well as tryptophans and represented the preferences by frequency plots (Fig. 6). According to Boltzmann, a frequency f_k at position k of a glucose is related by $f_k = c{\cdot}\exp(-\Delta H_k/RT)$ to the glucose binding energy ΔH_k, where c is a constant. This relation is rigorous for interactions between an isolated glucose and an isolated aromatic ring when based on observed frequencies of the isolated species. Since all statistics were done in proteins, however, we had to restrict the Boltzmann approach to dominant attractive ($\Delta H_k < 0$, $f_k > c$) interactions, i.e., to glucoses near to the aromatic rings. At more distant positions glucoses are involved in numerous other, stronger interactions with the protein. Accordingly, we considered the second contour levels of the frequency distributions of Figure 6 as the divide at $\Delta H_k = 0$, and neglected all interactions with f_k values below that.

The pathway of a permeating single glucose unit, as defined by the regular saccharide helix screwing through the orifice, was related to the three interacting aromatic rings by projecting the pyranose ring center onto the plane of Tyr41, Tyr6, and Trp426.

Table 1. *Statistics of noncovalently bound pyranoses to proteins as derived from the Protein Data Bank*

	Position of pyranose				
Type of pyranose	Trp[a]	Tyr[a]	Phe[a]	General	Total
All pyranoses[b]	28	17	11	22	78
Glucose[c]	13	10	5	9	37

[a] See Methods for the definition of the location.

[b] Except for sialic acids and phosphorylated sugars. The 78 entries of the Protein Data Bank (as of 24-April-1996) were: *1ABE*, *1ABR*, *1AFA*, *1AGM*, *1AGM*, *1BCX*, 1BFC, *1BTC*, 3*1BTC, *1BYH*, 3**1CDG*, 3**1CEN*, *1CGU*, *1CGV*, 1CHB, *1CHB*, 2**1CXE*, 2**1DBP*, *1DMB*, *1DRJ*, *1GCA*, 1GLG, *1HEW*, 1HEW, *1HGG*, *1HGG*, *1HLC*, 1HLC, 1HOT, 1HVQ, *1LMO*, *1LMT*, *1LED*, *1LES*, *1LTE*, 1LTE, *1LTT*, *1LZG*, 2**1MDP*, *1MDQ*, 2**1MFA*, *1MFB*, 1MSA, 1PNF, 2**1PPI*, *1PRI*, 1PTO, *1R1A*, 1RDN, *1SBA*, *1SLB*, *1TLF*, 1WGC, 3**1XIF*, 2**2AAI*, 2ACQ, *2GBP*, 2YHX, *5CNA*, 2**5GPB*, 3*5GPB, where Trp, Tyr, and Phe positions are *in italics* and glucoses are underlined. Multiplicities arise because some entries contain more than one sugar and some sugars bind to more than one aromatic ring.

[c] Either as monomer or as part of an oligosaccharide

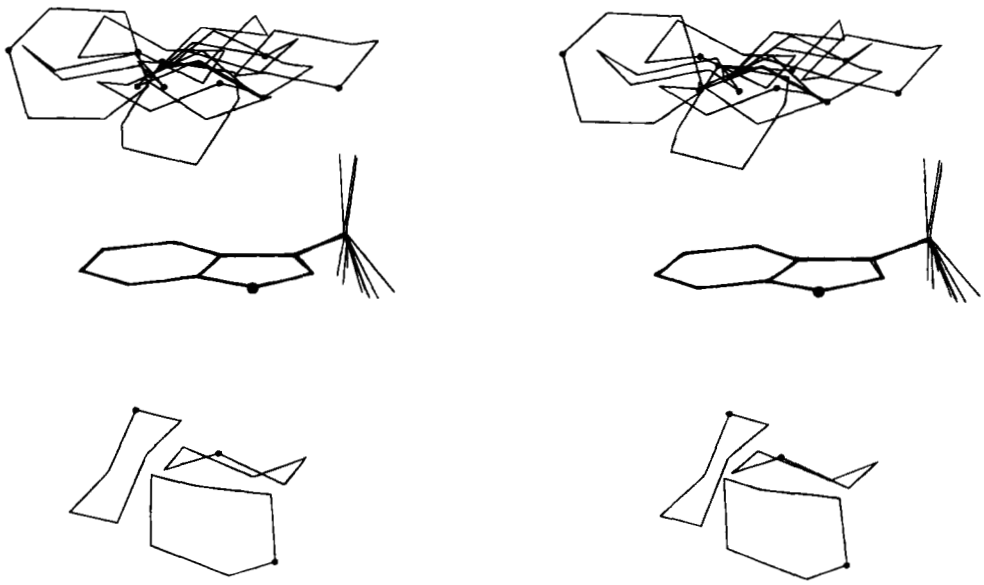

Fig. 5. Scatter plot of 13 independent entries in the Protein Data Bank showing glucoses (single or as part of an oligomer) bound at tryptophans. Only the pyranose ring atoms are depicted. Hetero atoms are marked.

This resulted in rather irregular trails shown in Figure 6. At each glucose position i we calculated ΔH_{ij} values by taking the logarithm of the frequency f_{ij} at each aromatic side chain j and adding them up to $\Delta H_i = \sum_j \Delta H_{ij}$, where ΔH_{ij} was taken as zero for all f_{ij} below the second contour level. This yielded the energy profile shown in Figure 7B, which has the second contour level as zero line.

In spite of the uncertainties of this approach, the profile shows clearly three binding energy minima that are displaced from the observed binding sites S1 to S3. Again the energy profile of the oligomer is derived by adding the single glucose profiles in proper register. The result is also shown in Figure 7B. The energy function becomes periodic as soon as G1 passes over S1, the minima occur about 0.4 units after the glucoses pass the binding sites.

Total energy profile

The binding energy contributions of the polar and the saccharide-aromatics interactions are added to yield Figure 7C. The resulting profile is rather smooth, because the optimal binding positions of both contributions are offset by about half a glucose unit, such that the minima of the saccharide-aromatics interactions (Fig. 7B) tend to compensate the maxima of the polar ones (Fig. 4B). The residual ripple is merely somewhat above ± 1 kJ/mol.

As a consequence, the oligomer does not encounter high energy hurdles hindering permeation as in a "ratchet type." Rather, permeation follows a "slide type" where the oligomer can move freely along the pore. The energy steps of initial binding and final dissociation are presumably decreased by weak binding sites (e.g., at Trp74′, Tyr227, and Trp368, Fig. 2) between orifice and both channel ends.

For relating the derived energy profile to the observed dissociation constant, we have to account for the entropy change on binding. On one hand, entropy disfavors binding because it fixes the oligosaccharide conformation, but on the other there is a favorable entropy contribution from the release of some bound water molecules (Meyer et al., 1997) to the bulk solvent. Taken together, we consider the entropy contribution to oligomer binding as negligible within the framework of our rough energy estimates and equate the binding enthalpies of Figure 7C with Gibbs free energies. Accordingly, the minimum level of the total binding energy profile of about -25 kJ/mol can be converted to a dissociation constant ranging somewhat below 1 mM, which is in general agreement with the experimental data of Schülein and Benz (1990).

In conclusion, the strong transversal electrostatic field of general porins (Weiss et al., 1991; Cowan et al., 1992; Schulz, 1993; Kreusch & Schulz, 1994) is replaced in maltoporin by hydrogen bonding partners offering almost continuous glucose-binding energy to a translocating maltooligosaccharide. The network of hydrogen bonding partners is stabilized by pairs of oppositely charged residues in the pore, i.e., Glu37-Arg33, Glu39-Arg8, Glu43-Arg82, Asp73'-Arg82, Asp116-Arg33, Glu218-Lys229, Glu424-Arg370. Despite the introduced inaccuracies, the shapes of the two energy profiles and especially the half-unit off-set between them are significant. Clearly, the saccharide-aromatics interactions flatten the spikes of the hydrogen bonding energy profile.

Methods

Translocation of maltooligosaccharide

The bound maltotrioside forms a regular helix which can be described by a rotation/translation. All putative intermediate glucose positions were determined by subdividing a full rotation/translation between G1 and G2 as well as between G2 and G3 into ten steps. An extension over both ends gave rise to further putative positions beyond sites S3 and S1, respectively. The evaluation of hydrogen bonds energies and hydrophobic energies was done manually at each position.

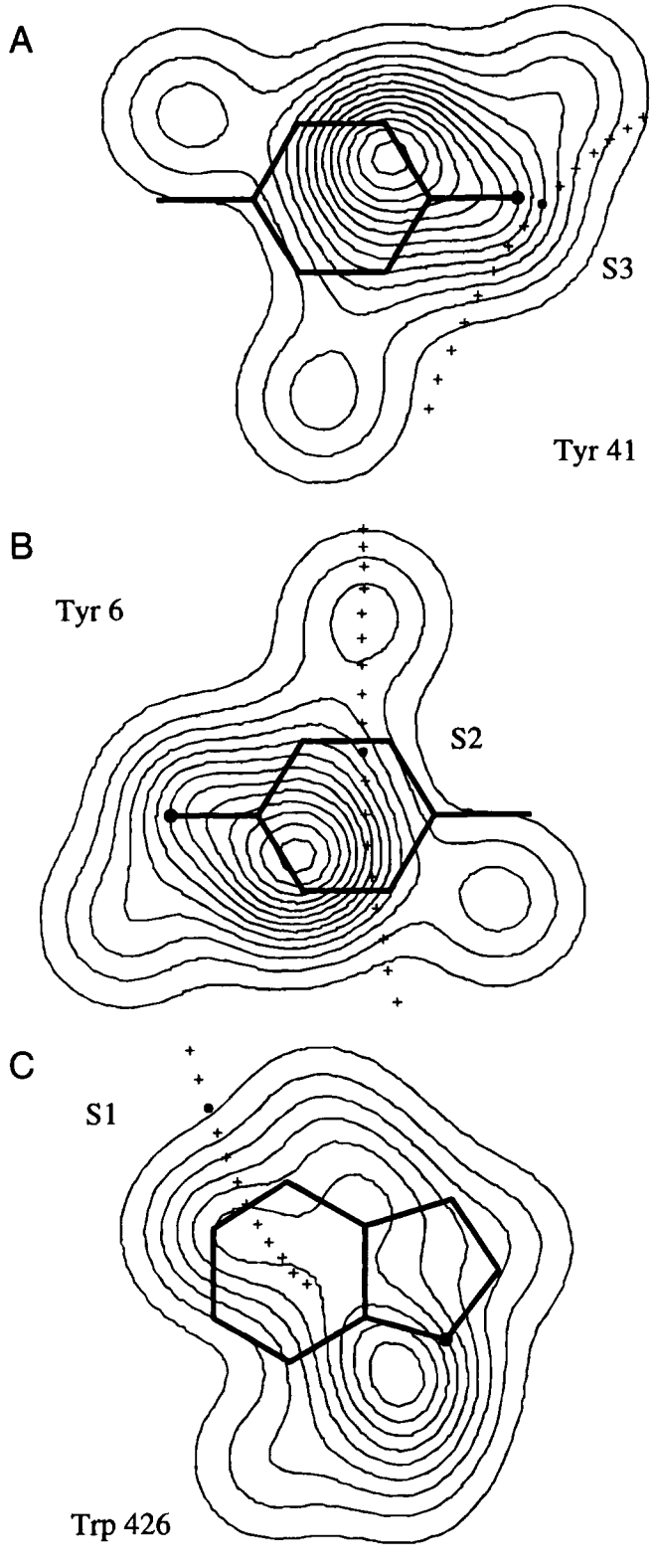

Fig. 6. Pathway of a glucose unit permeating the orifice by screwing along the regular saccharide helix. The path is projected onto the contacting aromatic rings of Tyr41, Tyr6, and Trp426. The observed binding sites S1, S2, and S3 are marked by dots. The path from one site to the next is subdivided into 10 equal steps giving rise to 9 further putative positions. Because the helix is regular, the putative positions could be extended beyond S3 and S1, respectively. The arrangement of the aromatic rings (hetero atoms marked) approximates their locations at the orifice (periplasm at the bottom), but they are separated such that all 8 putative glucose positions below S3 at Tyr41 are also present at Tyr6, and the last putative position below S2 at Tyr6 is also present at Trp426. For each of the three side chains the frequency distribution of glucose units as derived from the Protein Data Bank is given as a density distribution normalized to equal volume. The contours are at 10, 20, 30, etc. arbitrary units.

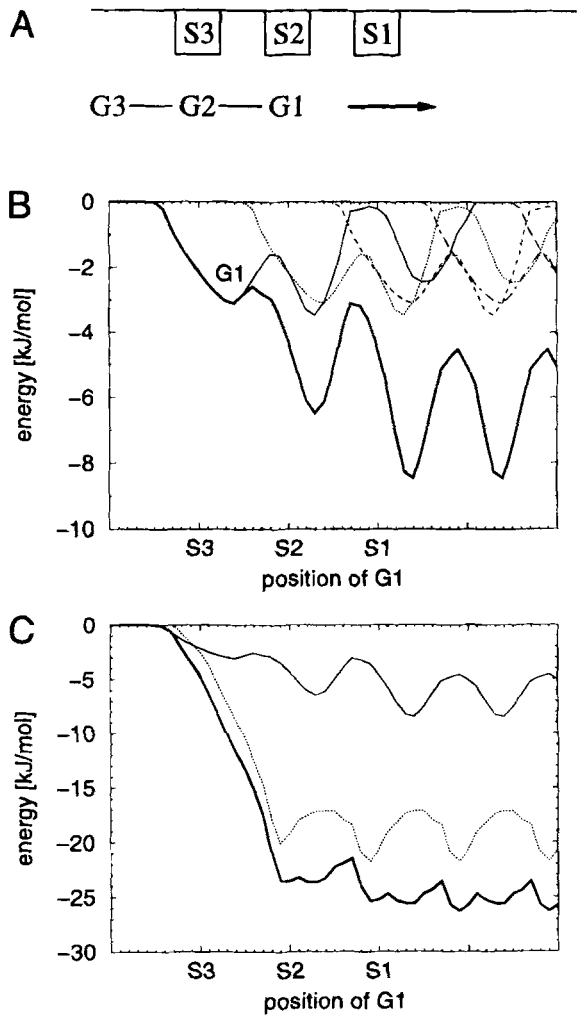

Fig. 7. Total energy profile of a maltooligosaccharide as it permeates maltoporin. **A:** Sketch of an oligomer passing over the observed binding sites S3, S2, and S1 toward the periplasm. **B:** Saccharide-aromatics interaction energy profiles of glucose units G1, G2, etc. (different line types) passing the side chains of Tyr41, Tyr6, and Trp426 at the orifice as derived from the frequency distributions of Figure 6 (see text). Appropriate addition yields the energy of a permeating oligomer (thick line), which becomes periodic as soon as G1 passes over S1. **C:** Combination of the hydrogen bonding energy profile (dotted line) from Figure 4B with the saccharide-aromatics energy profile (solid line) to yield the total energy profile (thick line). The minimum of this profile for the path of G1 up to S1 is close to S1, explaining the observed binding position of the maltotrioside (no G4, etc.).

Distribution of saccharide-binding sites in proteins

The Protein Data Bank (Bernstein et al., 1977) was screened for structures containing noncovalently bound pyranoses. These were related to the next aromatic ring of Phe, Tyr, or Trp. For each pair, we determined center P_i of the pyranose ring and center A_i of the aromatic ring atoms. A vertical distance was defined between point P_i and the aromatic plane. The lateral displacement was the distance between A_i and the projection of P_i onto the aromatic plane. A pyranose was considered to bind at an aromatic side chain if the vertical distance and the lateral displacement were below 5 Å and 4 Å, respectively. Otherwise, the binding site was considered as "general." There was a clear separation because only few cases were near the cut-off values. All pyranoses (except sialic acids and phosphorylated ones) were entered into Table 1.

When referred to the aromatic ring atoms as shown in Figure 5, the pyranoses align mostly parallel to the aromatic plane at a ring-to-ring distance of approximately 4.0 Å. The saccharides are mostly *trans* to the C_α atom, presumably because of steric hindrance by the main chain and neighboring residues. For the maltotrioside bound to maltoporin (Fig. 3) the vertical distances were 4.5 Å, 4.2 Å, and 4.1 Å for the G3:Tyr41, G2:Tyr6, and G1:Trp426 interactions, respectively. The corresponding lateral displacements were 3.1 Å, 1.1 Å, and 3.4 Å.

Probability of pyranose at tyrosines and tryptophans

As a first step, all centers P_i of the pyranoses were projected onto the aromatic ring planes of the reference tyrosine or tryptophan, respectively. Subsequently, a Gaussian function with a full width at half maximum of 2 Å was centered at each projected P_i. The probability function was then taken as the sum of all these Gaussians and normalized to equal volume (Fig. 6).

Acknowledgments

We thank M. Hofnung and A. Charbit for discussions. The project was supported by the Deutsche Forschungsgemeinschaft in the Graduiertenkolleg *Strukturbildung in Makromolekülen.*

References

Benz R, Schmid A, Nakae T, Vos-Scheperkeuter GH. 1986. Pore formation by LamB of *E. coli* in lipid bilayer membranes. *J Bacteriol 165*:978–986.

Bernstein FC, Koetzle TF, Williams GJ, Meyer EF, Brice MD, Rodgers JR, Kennard O, Shimanouchi T, Tasumi M. 1977. The protein data bank, a computer-based archival file for macromolecular structures. *J Mol Biol 112*:535–542.

Chakrabarti P, Samanta U. 1996. CH/π interaction in the packing of the adenine ring in protein structures. *J Mol Biol 251*:9–14.

Connolly ML. 1993. The molecular surface package. *J Mol Graphics 11*:139–141.

Cowan SW, Schirmer T, Rummel G, Steiert M, Gosh R, Pauptit RA, Jansonius JN, Rosenbusch JP. 1992. Crystal structures explain functional properties of two *E.coli* porins. *Nature 358*:727–733.

Dutzler R, Wang Y-F, Rizkallah PJ, Rosenbusch JP, Schirmer T. 1996. Crystal structures of various maltooligosaccharides bound to maltoporin reveal a specific sugar translocation pathway. *Structure 4*:127–134.

Goldsmith E, Sprang S, Fletterick R. 1982. Structure of maltoheptaose by difference Fourier methods and a model for glycogen. *J Mol Biol 156*:411–427.

Hinrichs W, Büttner G, Steifa M, Betzel C, Zabel V, Pfannemüller B, Saenger W. 1987. An amylose antiparallel double helix at atomic resolution. *Science 238*:205–208.

Kreusch A, Schulz GE. 1994. Refined structure of the porin from *Rhodopseudomonas blastica* and comparison with the porin from *Rhodobacter capsulatus*. *J Mol Biol 243*:891–905.

Luckey M, Nikaido H. 1980a. Specificity of diffusion channels produced by lambda phage receptor protein of *Escherichia coli*. *Proc Natl Acad Sci USA 77*:167–171.

Luckey M, Nikaido H. 1980b. Diffusion of solutes through channels produced by phage lambda receptor protein of *Escherichia coli*: Inhibition by higher oligosaccharides of the maltose series. *Biochem Biophys Res Commun 93*:166–171.

Meyer JEW, Hofnung M, Schulz GE. 1997. Structure of maltoporin from *Salmonella typhimurium* ligated with a nitrophenyl-maltotrioside. *J Mol Biol.* In press.

Nikaido H. 1994. Porins and specific diffusion channels in bacterial outer membranes. *J Biol Chem 269*:3905–3908.

Quiocho FA. 1989. Protein-carbohydrate interactions: Basic molecular features. *Pure Appl Chem 61*:1293–1306.

Schirmer T, Keller TA, Wang Y-F, Rosenbusch JP. 1995. Structural basis for sugar translocation through maltoporin channels at 3.1 Å resolution. *Science 267*:512–514.

Schülein K, Benz R. 1990. LamB (maltoporin) of *Salmonella typhimurium*: Isolation, purification and comparison of sugar binding with LamB of *Escherichia coli*. *Molec Microbiol 4*:625–632.

Schulz GE. 1993. Bacterial porins: structure and function. *Curr Opin Cell Biol 5*:701–707.

Thirion JP, Hofnung M. 1972. On some genetic aspects of phage λ resistance in *E. coli* K12. *Genetics 71*:207–216.

Weis WI, Drickamer K. 1996. Structural basis of lectin-carbohydrate recognition. *Annu Rev Biochem 65*:441–473.

Weiss MS, Abele U, Weckesser J, Welte W, Schiltz E, Schulz GE. 1991. Molecular architecture and electrostatic properties of a bacterial porin. *Science 254*:1627–1630.

Weiss MS, Wacker T, Weckesser J, Welte W, Schulz GE. 1990. The three-dimensional structure of porin from *Rhodobacter capsulatus* at 3 Å resolution. *FEBS Lett 267*:268–272.